RSC Advances

PAPER

View Article Online
View Journal | View Issue

Cite this: *RSC Adv.*, 2022, **12**, 6841

Computational screening of transition-metal doped boron nanotubes as efficient electrocatalysts for water splitting†

Jiajie Lu,[a] Xiuli Hou, *[a] Beibei Xiao,[b] Xuejian Xu,[a] Jianli Mi[a] and Peng Zhang[ac]

Received 27th December 2021
Accepted 22nd February 2022

DOI: 10.1039/d1ra09381a

rsc.li/rsc-advances

The search for efficient and low-cost electrocatalysts for the oxygen evolution reaction (OER) and the hydrogen evolution reaction (HER) is of utmost importance for the production of hydrogen and oxygen *via* water splitting. In this work, the catalytic performance of the OER and HER on transition metal doped boron nanotubes (BNTs) was investigated using density functional theory. It was found that the doped transition metal atoms determine the catalytic activity of the BNTs. Rhodium-doped BNTs exhibited excellent OER activity, while cobalt-doped BNTs displayed great catalytic activity toward the HER. Volcano relationships were found between the catalytic activity and the adsorption strength of reaction intermediates. Rhodium- and cobalt-doped BNTs exhibited great OER and HER catalytic activity due to the favorable adsorption strength of reaction intermediates. This work sheds light on the design of novel electrocatalysts for water splitting and provides helpful guidelines for the future development of advanced electrocatalysts.

Introduction

Due to the dwindling global reserves of fossil fuels and the harmful effects of greenhouse gases, the development of alternative clean energy fuels has been considered as one of the most concerning topics in the past few decades.[1] Hydrogen is expected to be a clean energy alternative to traditional fossil fuels due to its high energy density and lack of carbon emissions.[2–4] Among current hydrogen production technologies, producing hydrogen through electrochemical water splitting has received an increasing level of attention due to the absence of environmental pollution compared with other methods such as steam reforming and coal gasification. Electrochemical water splitting can be divided into two half-reactions: the oxygen evolution reaction (OER) at the anode side and the hydrogen evolution reaction (HER) at the cathode side. Both half-reactions require highly active electrocatalysts to accelerate the reaction process and reduce the overpotential.[5,6] Presently, the commonly used HER and OER electrocatalysts are the noble metal platinum (Pt) and noble metal oxides such as ruthenium dioxide (RuO_2) and iridium dioxide (IrO_2).[6] However, these materials are scarce and expensive, which severely limits their large-scale application.[7] Therefore, during the last few decades, numerous efforts have been devoted to find the low-cost and non-noble metal electrocatalysts for electrochemical water splitting.

Single-atom catalysts (SACs) consist of dispersed single metal atoms and a support species. These catalysts make the most efficient use of metal atoms to significantly enhance the catalytic activity.[8–10] Lv *et al.* evaluated the HER and OER catalytic performance of holey graphitic carbon nitride (g-CN) supported transition metal (TM) atoms (Ti, V, Cr, Mn, Fe, Co and Ni) based on density functional theory (DFT) and found that Co_1/g-CN and Ni_1/g-CN exhibited the best catalytic activity with HER/OER overpotentials of 0.15/0.61 and 0.12/0.40 V, respectively.[11] Ling *et al.* Also reported that isolated nickel atoms supported on a β_{12} boron monolayer (Ni_1/β_{12}-BM) achieved water splitting with overpotentials of 0.40 V for OER and 0.06 V for HER based on DFT calculations.[12] Li *et al.* successfully activate an inefficient OER catalyst by a simple atom tailoring strategy and found that the achieved SACs (Cu_2O-RhSA) exhibited significantly enhance catalytic activity toward OER in alkaline media in experiment.[13] Liu *et al.* reported that single-site Co in a well-defined brookite TiO_2 nanorod (210) surface presents turnover frequencies that are among the highest for Co-based heterogeneous catalysts in experiment.[14] These results show that SACs supported by various nanostructures can exhibit excellent catalytic activity and reduce the cost of the catalyst.

Carbon nanotubes (CNTs) have been proved to be an excellent support for SACs due to their unique physical and chemical

[a]*Institute for Advanced Materials, School of Materials Science and Engineering, Jiangsu University, Zhenjiang 212013, China. E-mail: houxiuli@ujs.edu.cn*

[b]*School of Energy and Power Engineering, Jiangsu University of Science and Technology, Zhenjiang 212003, China*

[c]*Key Laboratory for Water Quality and Conservation of the Pearl River Delta, Ministry of Education, Institute of Environmental Research at Greater Bay, Guangzhou University, Guangzhou 510006, China*

† Electronic supplementary information (ESI) available. See DOI: 10.1039/d1ra09381a

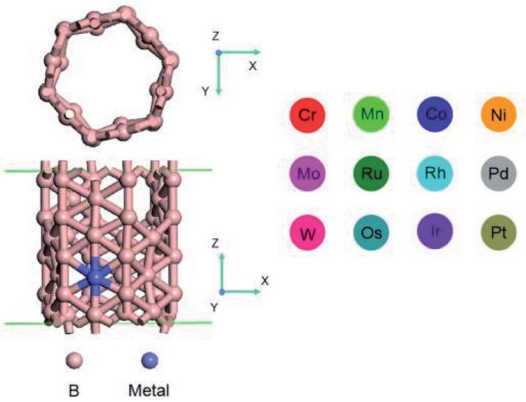

Fig. 1 Atomic structure of transition metal-doped BNTs.

properties. From the perspective of conductivity, CNTs are usually divided into three types: metal, semiconductor, and insulator, which results from the chirality and leads to a large difference in the electrical conductivity of CNTs.[15–17] In order to overcome the large differences in the conductivity of CNTs, many investigations have been performed to find new alternative nanotube materials with consistent electronic properties. In recent studies, alternative nanotubes containing pure elements (B, Au, Si) have been successfully synthesized, which have consistent electronic properties.[18–20] Boron is close to carbon in the periodic table and it is one of the few elements that has independent monolayer allotropes. Boron-based structures exhibit special chemical and physical properties, such as low density, high melting point, excellent chemical stability, high thermal and electrical conductivity.[21–31] Theoretical calculations indicate that the density of states (DOS) of boron nanotubes (BNTs) is similar to that of metal, showing its excellent metal properties.[32] Individual BNTs also exhibit excellent field emission properties, with a high stable current of approximately 80 μA and a current density close to that of CNTs (2×10^{11} A m^{-2}).[31] The pore structure of BNTs is uniform and stable, which can act as the adsorption site for transition metal atoms. The special physical and chemical characteristics of BNTs indicates that BNT may be a promising support for SACs.[14,33] However, if the BNTs can act as a good substrate in SACs for OER and HER is unclear.

In this work, the catalytic activity of twelve transition metal (Cr, Co, Ir, Mn, Mo, Ni, Os, Pd, Pt, Rh, Ru and W) doped BNTs for OER and HER was systematically investigated using DFT calculations (Fig. 1). It was found that the central transition metal atom determines the catalytic activity of OER and HER. Volcano-type curves were found between the catalytic activity and adsorption strength of the reaction intermediates. Among the 12 TM-doped BNTs, Rh/BNTs exhibited the best OER catalytic activity and Co/BNTs displayed the best HER catalytic activity.

Computational methods

All calculations were performed within DFT framework by DMol³ code.[34] The generalized gradient approximation (GGA) with PW91 was selected as the exchange and correlation functionals.[35] The all-electron relativistic method was selected for core treatment, which includes all electrons explicitly and introduces some relativistic effects into the core.[36] Double numerical plus polarization (DNP) was selected as the basis set.[37] A smearing value of 0.005 Ha was used to accelerate the electronic convergence. The actual truncation radius was set as 5.2 Å. The van der Waals (vdW) interaction is very important for the adsorption of the adsorbate on the substrate.[38] In order to describe the vdW interaction, the DFT + vdW method within the Grimme scheme was employed.[39–41] The convergence tolerances of energy, maximum displacement and displacement were 1.0×10^{-5} Ha, 0.005 Å, and 0.002 Ha/Å, respectively. The convergence tests for truncation radius and energy convergence tolerance was shown in Tables S1 and S2 of ESI.† The vacuum layer was set to 20 Å to eliminate the interaction between two periodic images.

In this work, the catalytic activity of BNTs doped with 12 different transition metal atoms (Co, Cr, Ir, Mn, Mo, Ni, Os, Pd, Pt, Rh, Ru and W) for water splitting was systematically investigated. Previous work has shown that α-SWBNTs are all metallic, regardless of their diameter and chirality.[42] Therefore, in this work, (6,0) zigzag α-SWBNT with one single cell was used to describe the structure of born nanotube. The optimized lattice constants for Co-, Cr-, Ir-, Mn-, Mo-, Ni-, Os-, Pd-, Pt-, Rh-, Ru- and W-doped BNTs were $26 \times 26 \times 6.76$, $26 \times 26 \times 6.76$, $26 \times 26 \times 6.79$, $26 \times 26 \times 6.77$, $26 \times 26 \times 6.76$, $26 \times 26 \times 6.79$, $26 \times 26 \times 6.75$, $26 \times 26 \times 6.79$, $26 \times 26 \times 6.8$, $26 \times 26 \times 6.79$, $26 \times 26 \times 6.77$ and $26 \times 26 \times 6.75$ $Å^3$, respectively. During the process of water splitting, O_2 was produced on the anode side *via* the $4e^-$ pathway and H_2 was produced on the cathode side *via* the $2e^-$ pathway. For the OER reaction on the anode side, the elemental reaction steps can be written as:

$$H_2O(l) + * \rightarrow OH^* + H^+ + e^-$$

$$OH^* \rightarrow O^* + H^+ + e^-$$

$$O^* + H_2O \rightarrow OOH^* + H^+ + e^-$$

$$OOH^* \rightarrow O_2(g) + H^+ + e^-$$

For the HER reaction occurring on the cathode side, the basic reaction steps can be written as:

$$2H^+ + 2e^- \rightarrow H^* + H^+ + e^- \rightarrow H_2(g)$$

The adsorption energy (E_{ad}) of the reaction intermediates on TM/BNT was calculated as:

$$E_{ad} = E_{mol\text{-}TM/BNTs} - E_{mol} - E_{TM/BNTs} \quad (1)$$

where E_{mol}, $E_{TM/BNTs}$, and $E_{mol\text{-}TM/BNTs}$ represent the electronic energies of the isolated molecule, the TM-doped BNTs and the adsorption system, respectively.[38,43,44] Based on this definition, a negative E_{ad} value indicates an exothermic adsorption

process. The reaction free energy (ΔG) of each elemental step in the OER and HER processes was calculated based on the computational hydrogen electrode (CHE) model.[45] The ΔG value was calculated as:

$$\Delta G = \Delta E + \Delta \mathrm{ZPE} + \Delta \int C_\mathrm{p} \mathrm{d}T - T\Delta S \quad (2)$$

where ΔE was the change in total energy determined by the DFT calculations, ΔZPE was the change of the zero-point energy, $\Delta \int C_\mathrm{p} \mathrm{d}T$ was the contribution of heat capacity, ΔS was the change of entropy and T represented temperature (298.15 K in this case).[10,46] The calculated free energy corrections were summarized in Tables S3 and S4.† The OER overpotential (η) was calculated with Nørskov's assumption:[47]

$$\eta = \Delta G_\mathrm{max}/\mathrm{e} - 1.23\ \mathrm{V} \quad (3)$$

The aqueous environment was represented by the conductor-like screening model (COSMO), and the dielectric constant of the solvent was set to 78.54.

Results and discussion

The catalytic activity of pristine BNTs was first checked. Three different adsorption sites of pristine BNTs were considered here. Fig. 2 shows the Gibbs free energy diagrams of the OER and HER on pristine BNTs with three different adsorption sites. The adsorption structures of reaction intermediates on BNTs were summarized in Fig. S1 of ESI.† The overpotential values of OER were calculated to be 1.50, 1.56, and 2.50 V, respectively, and the overpotential values of HER were calculated as 0.26, 1.00, and 0.36 V. It is clear that the overpotential values of pristine BNTs are significantly higher than the benchmark overpotentials of RuO_2 (0.56 V) and Pt (0.09 V),[47,48] indicating that the catalytic activity of pristine BNTs is not as good as RuO_2 or Pt.

Doping is one of the promising strategies to modify the electronic structure of catalyst by changing the composition of the active site. Introducing heterogeneous atoms into the surface of catalysts can significantly enhance the catalytic performance. In order to further improve the catalytic activity of the BNTs, the effect of dopants on the catalytic activity of BNTs was investigated.

In the following step, the adsorption of free transition metal atoms on BNTs was calculated. The adsorption energies are summarized in Table S5.† The more negative the adsorption energy is, the more stable the adsorption is. As shown in Table S5,† the transition metal atoms can adsorb on the vacancy site of BNTs stably. In other word, the vacancy of BNTs can anchor the free transition metal atoms stably. Furthermore, the adsorption energies of metal atoms on BNTs respect to bulk metal were also calculated (shown in Table S6 of ESI†). Obviously, the values are larger than those based on free metal atoms.

According to the Sabatier principle, the favorable adsorption of the reaction intermediate on the surface of a catalyst is a prerequisite for the catalytic reaction.[49] Therefore, the adsorption energies of the reaction intermediates on different TM-doped BNTs were calculated and summarized in Table S7.† It was found that the adsorption energy of the reaction intermediates gradually decreased as the TMs varying from group 6 to group 10. As the adsorption strength of reaction intermediates determines the catalytic activity, the different adsorption properties of the reaction intermediates on the TM-doped BNTs will lead to different reaction kinetics. Furthermore, scaling

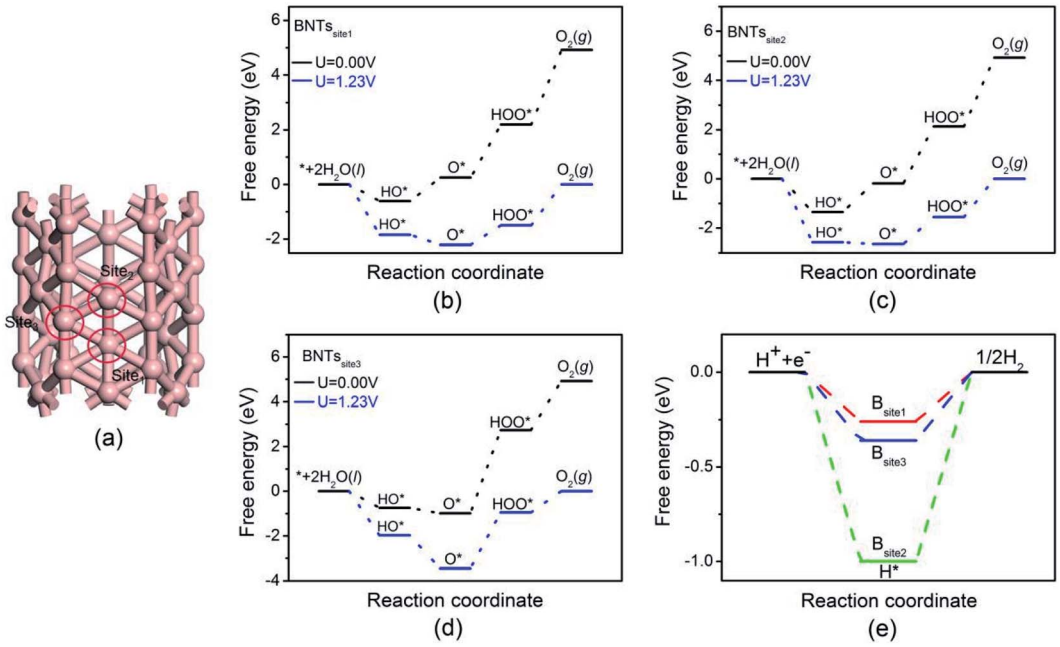

Fig. 2 Adsorption sites of pristine BNTs (a), free energy diagrams for the OER on pristine BNTs with site1 (b), site2 (c), and site3 (d), and free energy diagram for the HER on pristine BNTs (e).

relationships between the reaction intermediates were found. Three nearly linear relationship were observed between $E_{ad\text{-}OH}$, $E_{ad\text{-}O}$, and $E_{ad\text{-}OOH}$ (Fig. 3). The fitting equations are as follow:

$$E_{ad\text{-}O} = 1.34\ E_{ad\text{-}OOH} - 1.87 \quad (4)$$

$$E_{ad\text{-}OH} = 0.58\ E_{ad\text{-}OOH} - 2.19 \quad (5)$$

$$E_{ad\text{-}OH} = 0.44\ E_{ad\text{-}O} - 1.35 \quad (6)$$

Where, the coefficient of determination values are 0.94, 0.87, and 0.95, respectively. Therefore, the adsorption energy of OOH can be used as a descriptor to characterize the catalytic activity of the OER reaction. As shown in Fig. S2 of ESI,† the reaction intermediates of OER adsorb an the top site of the doped transition metal atoms. The TM–O bond controls the adsorption strength of the OER intermediates. The transition metal atoms are the active centers for OER. The intrinsic property of transition metal atoms determines the adsorption strength of OER intermediates, and then results in the scaling relationships between the reaction intermediates. The first ionization energy, which is defined as the amount of energy needed to remove an electron from an isolated atom, represents an intrinsic property of elements. As shown in Fig. 3(c), scaling relationships were also found between the first ionization energy and the adsorption energies of the OER intermediates. Generally, the smaller the first ionization energy, the stronger the adsorption of the OER intermediates is.

The thermodynamic potential of water oxidation to produce oxygen under standard conditions is 1.23 V. In the case of an ideal catalyst, the ΔG of the four coupled proton and electron transfer (CPET) steps is 1.23 eV. However, in practice, there is at least one CPET step with a ΔG value larger than 1.23 eV. Fig. 4 shows the Gibbs free energy diagrams of OER on 12 different TM-doped BNTs. As can be seen, the potential-determining step of Cr-, Mn-, Co-, Mo-, W-, Os- and Pt-doped BNTs is the last step (the decomposition of OOH), leading to ΔG values of 3.66, 2.71, 1.80, 3.57, 4.87, 3.37 and 2.37 eV, respectively. The formation of OOH is the potential-determining step for Ru-, Rh- and Ir-doped BNTs, with ΔG values of 2.32, 1.79 and 2.39 eV, respectively. The potential-determining step of Ni- and Pd-doped BNTs is the second step (the decomposition of OH), with ΔG values of 1.88 and 2.07 eV, respectively. The Gibbs free energy diagram shows that Rh-doped BNTs exhibit the highest OER catalytic activity due to the smallest reaction free energy of the potential-determining step and the smallest overpotential (0.56 V).

A volcano curve exists between the overpotential and the adsorption energy of the OOH intermediate species ($E_{ad\text{-}OOH}$). As shown in Fig. 5, the volcano curve can be divided into two regions. Pd- and Rh-doped BNTs are located on the left branch, while Co-, Ni-, Ru-, Ir-, Pt-, Mn-, Os-, Cr-, Mo- and W-doped BNTs are located on the right branch. For Mn-, Os-, Cr-, Mo- and W-doped BNTs, that located in the outlying right region of the volcano curve, the strong adsorption energy of OER intermediates makes it difficult to renew the catalysts and the active site is easily poisoned. Rh-doped BNTs are located at the top of the volcano

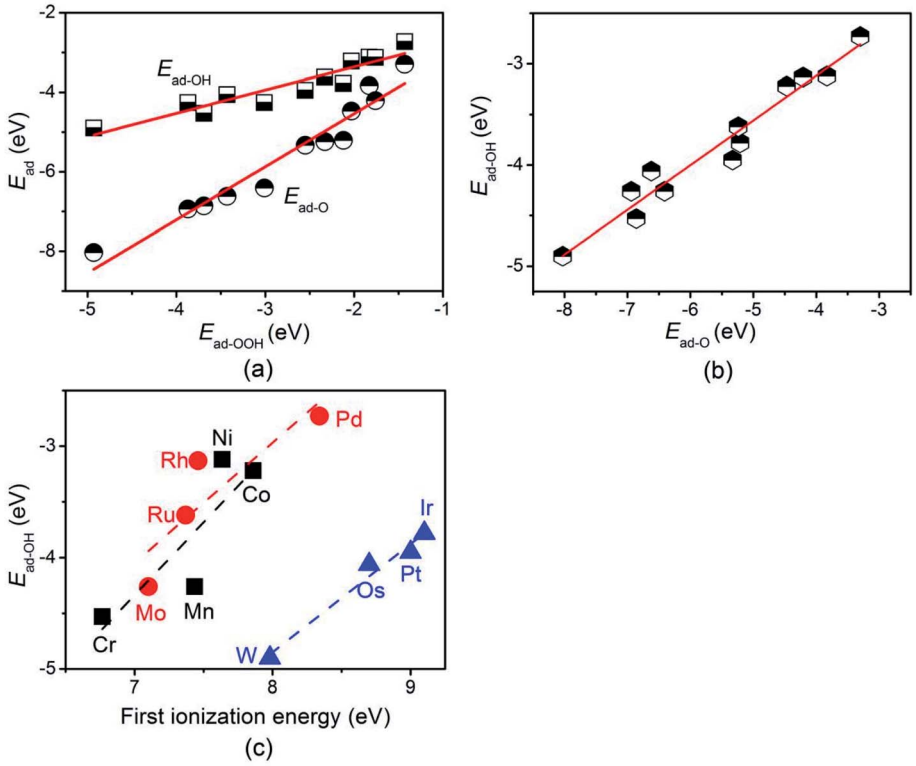

Fig. 3 The relationship between the adsorption energy of OOH, O, and OH on TM-doped BNTs (a) and (b), the relationship between the adsorption energy of OH and the first ionization energy (c).

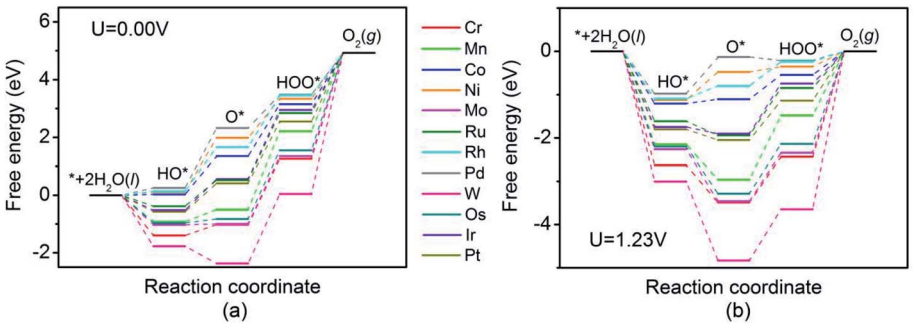

Fig. 4 Gibbs free energy diagram of the OER on TM-doped BNTs.

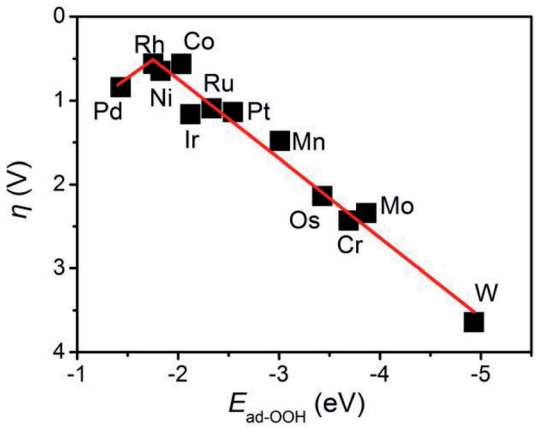

Fig. 5 The volcano relationship between the E_{ad} of OOH and the overpotential of the rate-determining step of the OER on TM-doped BNTs.

curve due to the favorable adsorption energies of the reaction intermediates, indicating that Rh-doped BNTs display the best OER catalytic activity among the twelve TM-doped BNTs.

Next, the HER catalytic performance of TM-doped BNTs was studied. The Gibbs free energy diagram of HER was shown in Fig. 6(a). The adsorption structure of H atom on TM-doped BNTs were summarized in Fig. S3.† It was found that the Gibbs free energies for the reduction of H^+ on Co-, Ni-, Pd-, Rh-, Mo-, Ru-, Ir-, Cr-, Mn-, Pt-, Os- and W-doped BNTs were −0.02, −0.05, −0.06, −0.18, −0.24, −0.26, −0.59, −0.76, −0.79, −0.81, −0.89 and −0.98 eV, respectively. The overpotential values of HER on Co-, Ni-, and Pd-doped BNTs are smaller than those on other TM-doped BNTs, indicating that Co-, Ni-, and Pd-doped BNT catalysts can exhibit better HER catalytic activity. The overpotential of HER on Co/BNTs is very small (only 0.02 V), indicating excellent HER catalytic performance. The adsorption energy of H also plays an important role in the activity of HER. As shown in Fig. 6(b), a volcano relationship also was found between the overpotential of HER and the adsorption of H on TM-doped BNTs. Co/BNTs display the best catalytic activity due to the optimum adsorption energy of H. Note that the volcano relationship for HER on TM-doped BNTs in this work is different from the classical volcano curve for transition metal catalysts, where Pt exhibits the best HER catalytic activity.[50] This is because TM-doped BNTs can be characterized as single atom catalysts and the transition metal atoms in TM-doped BNTs are separated, which results in different electronic structures compared with bulk transition metals. Recently published works have shown that the adsorbates from the electrolyte can adsorb on the active site and play a important role in the catalytic activity.[51,52] In this work, the HER process *via* H_2O on Co-doped BNTs, which exhibit the best HER catalytic activity with the Volmer–Heyrovsky mechanism, was considered. As shown in Fig. S4,† the free energy for HER process *via* H_2O is 1.06 eV, which is very high to overcome, indicating that HER process on Co-doped BNTs prefers to through Volmer–Heyrovsky mechanism.

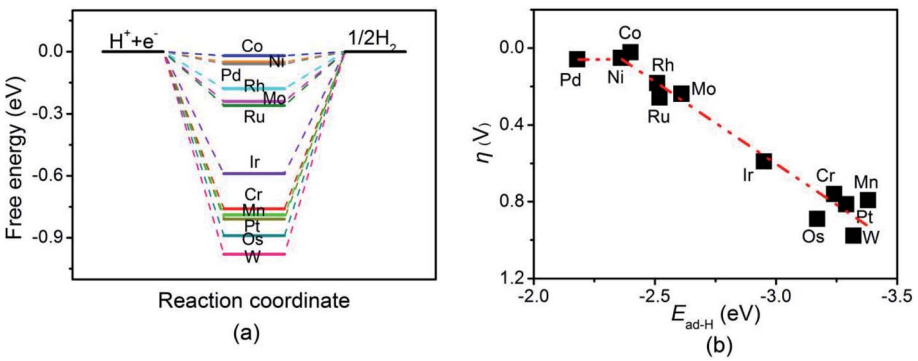

Fig. 6 (a) Gibbs free energy diagram of the HER on TM-doped BNTs, (b) the volcano relationship between the E_{ad} of H and the overpotential of HER on TM-doped BNTs.

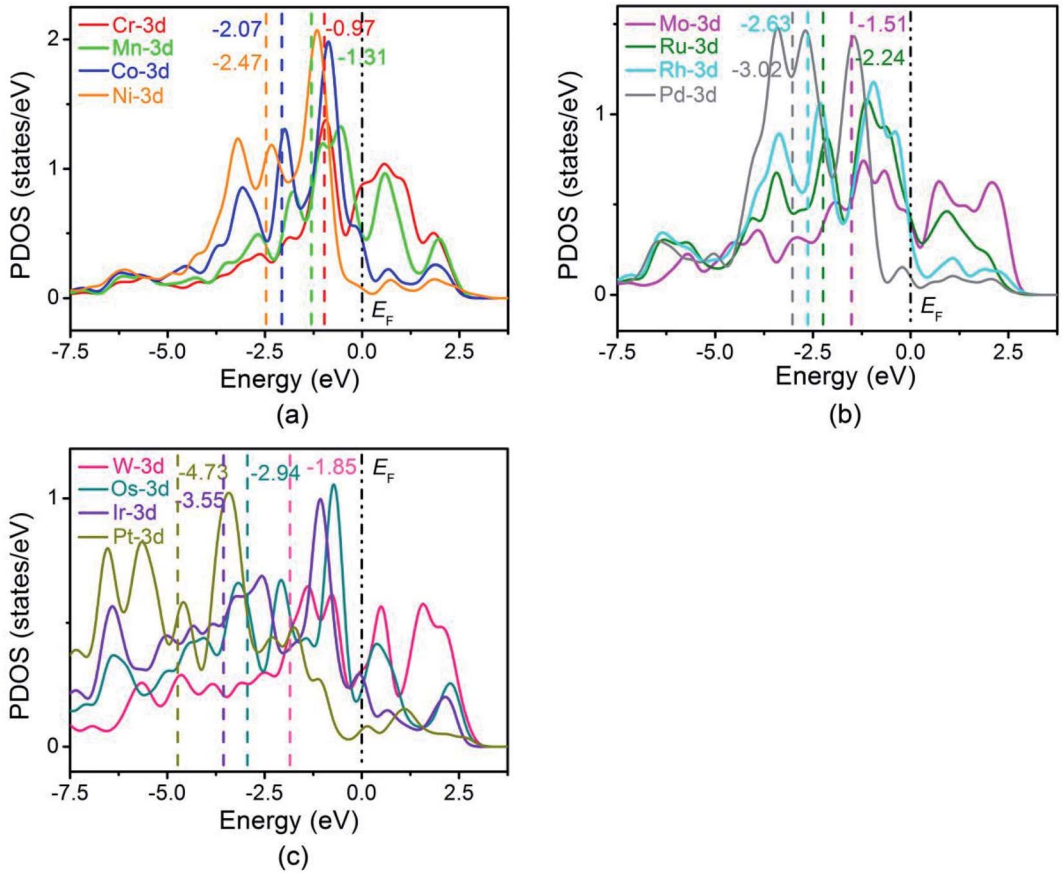

Fig. 7 The partial density of states (PDOS) of the transition metal doped BNTs.

It is well-known that the catalytic activity of catalysts is determined by the adsorption strength of the intermediates, which can be affected by the surface electronic states of the catalysts. In order to further explore the origin of the interaction between the reaction intermediates and the TM-doped BNTs, the electronic structures of three TM-doped BNTs were investigated. The partial density of states (PDOS) of transition metal doped BNTs are shown in Fig. 7. The relative reaction performance of the catalyst surface is reflected by the position of the d-band center, which can be understood as the average energy of d electrons (dividing the total energy by the number of electrons to get the average energy of d electrons).[53] As can be seen from Fig. 7, the d-band center is shifted to the left relative to the Fermi level as the central metal varying from left to right in a period, which results in a downward shift of the antibonding states and leads to a decrease in the adsorption energy of the intermediate on the central metal atom. This is consistent with the adsorption energies of the reaction intermediates in Table S7.† The PDOS states based on GGA + U approach were also calculated, as shown in Fig. S5.† Although the calculated d-band center values of transition metals based on the GGA + U method are different from those based on GGA approach, they show the similar trend.

Conclusions

In this work, the catalytic performance of TM-doped (Cr, Co, Ir, Mn, Mo, Ni, Os, Pd, Pt, Rh, Ru and W) BNTs as a new type of water electrolysis catalyst was investigated using DFT calculations. It was found that the catalytic performance of OER and HER is closely related to the doped TM atoms. Co/BNTs exhibit the best HER catalytic activity with an overpotential of only 0.02 V. For OER, the catalytic activity of Rh/BNTs was significantly higher than other TM-doped BNTs. This work provides insight into OER and HER reaction mechanisms on TM-doped BNTs and provides guidance for the design of high-performance water electrolysis catalysts.

Conflicts of interest

There are no conflicts to declare.

Acknowledgements

This work was supported by the financial support from the National Natural Science Foundation of China (Grant no. 21403092).

References

1 C. Zhao, W. Gao and Q. Jiang, *J. Phys. Chem. C*, 2020, **124**, 25412–25420.
2 J. A. Turner, *Science*, 2004, **305**, 972–974.
3 M. Balat, *Int. J. Hydrogen Energy*, 2008, **33**, 4013–4029.
4 S. Chu and A. Majumdar, *Nature*, 2012, **488**, 294–303.
5 X. Zou and Y. Zhang, *Chem. Soc. Rev.*, 2015, **44**, 5148–5180.
6 C. Zhu, Q. Shi, S. Feng, D. Du and Y. Lin, *ACS Energy Lett.*, 2018, **3**, 1713–1721.
7 C. C. Yang, S. F. Zai, Y. T. Zhou, L. Du and Q. Jiang, *Adv. Funct. Mater.*, 2019, **29**, 1901949.
8 H. Xu, S. Ci, Y. Ding, G. Wang and Z. Wen, *J. Mater. Chem. A*, 2019, **7**, 8006–8029.
9 H. Li, Y. Wu, L. Li, Y. Gong, L. Niu, X. Liu, T. Wang, C. Sun and C. Li, *Appl. Surf. Sci.*, 2018, **457**, 735–744.
10 Y. Wu, C. Li, W. Liu, H. Li, Y. Gong, L. Niu, X. Liu, C. Sun and S. Xu, *Nanoscale*, 2019, **11**, 5064–5071.
11 X. Lv, W. Wei, H. Wang, B. Huang and Y. Dai, *Appl. Catal., B*, 2020, **264**, 118521.
12 C. Ling, L. Shi, Y. Ouyang, X. C. Zeng and J. Wang, *Nano Lett.*, 2017, **17**, 5133–5139.
13 F. Li, G. F. Han, J. P. Jeon, T. J. Shin, Z. Fu, Y. Lu and J. B. Baek, *ACS Nano*, 2021, **15**, 11891–11897.
14 C. Liu, J. Qian, Y. Ye, H. Zhou, C. J. Sun, C. Sheehan, Z. Zhang, G. Wan, Y. S. Liu, J. Guo, S. Li, H. Shin, S. Hwang, T. B. Gunnoe, W. A. Goddard III and S. Zhang, *Nat. Catal.*, 2021, **4**, 36–45.
15 M. S. Dresselhaus, G. Dresselhaus and A. Jorio, *Annu. Rev. Mater. Res.*, 2004, **34**, 247–278.
16 J. W. G. Wildoer, L. C. Venema, A. G. Rinzler, R. E. Smalley and C. Dekker, *Nature*, 1998, **391**, 59–62.
17 T. W. Odom, J.-L. Huang, P. Kim and C. M. Lieber, *Nature*, 1998, **391**, 62–64.
18 D. Ciuparu, R. F. Klie, Y. Zhu and L. Pfefferle, *J. Phys. Chem. B*, 2004, **108**, 3967–3969.
19 R. T. Senger, S. Dag and S. Ciraci, *Phys. Rev. Lett.*, 2004, **93**, 196807.
20 X. Yang and J. Ni, *Phys. Rev. B: Condens. Matter Mater. Phys.*, 2005, **72**, 195426.
21 J. Zhang and J. Zhou, *Phys. E*, 2021, **127**, 114520.
22 R. R. Li, P. D. Dapkus, M. E. Thompson, W. G. Jeong, C. Harrison, P. M. Chaikin, R. A. Register and D. H. Adamson, *Appl. Phys. Lett.*, 2000, **76**, 1689–1691.
23 H. Tang and S. Ismail-Beigi, *Phys. Rev. Lett.*, 2007, **99**, 115501.
24 A. Gindulytė, W. N. Lipscomb and L. Massa, *Inorg. Chem.*, 1998, **37**, 6544–6545.
25 I. Boustani, A. Quandt, E. Hernández and A. Rubio, *J. Chem. Phys.*, 1999, **110**, 3176–3185.
26 I. Boustani, *Phys. Rev. B: Condens. Matter*, 1997, **55**, 16426–16438.
27 J. Niu, B. K. Rao and P. Jena, *J. Chem. Phys.*, 1997, **107**, 132–140.
28 X. Yang, Y. Ding and J. Ni, *Phys. Rev. B: Condens. Matter*, 2008, **77**, 041402.
29 X. Yu, L. Li, X.-W. Xu and C.-C. Tang, *J. Phys. Chem. C*, 2012, **116**, 20075–20079.
30 A. K. Singh, A. Sadrzadeh and B. I. Yakobson, *Nano Lett.*, 2008, **8**, 1314–1317.
31 F. Liu, C. Shen, Z. Su, X. Ding, S. Deng, J. Chen, N. Xu and H. Gao, *J. Mater. Chem.*, 2010, **20**, 2197–2205.
32 T. Thurn-Albrecht, J. Schotter, G. A. Kästle, N. Emley, T. Shibauchi, L. Krusin-Elbaum, K. Guarini, C. T. Black, M. T. Tuominen and T. P. Russell, *Science*, 2000, **290**, 2126–2129.
33 I. Boustani, *Chem. Modell.*, 2011, **8**, 1–44.
34 B. Delley, *J. Chem. Phys.*, 2000, **113**, 7756–7764.
35 J. P. Perdew, K. Burke and M. Ernzerhof, *Phys. Rev. Lett.*, 1996, **77**, 3865–3868.
36 D. D. Koelling and B. N. Harmon, *J. Phys. C: Solid State Phys.*, 1997, **10**, 3107–3114.
37 B. Delley, *J. Chem. Phys.*, 1990, **92**, 508–517.
38 W. Liu, A. Tkatchenko and M. Scheffler, *Acc. Chem. Res.*, 2014, **47**, 3369–3377.
39 S. Grimme, *J. Comput. Chem.*, 2006, **27**, 1787–1799.
40 P. Zhang, Z. Wang, L. Liu, L. H. Klausen, Y. Wang, J. Mi and M. Dong, *Appl. Mater. Today*, 2019, **14**, 151–158.
41 P. Lazar, F. Karlický, P. Jurečka, M. Kocman, E. Otyepková, K. Šafářová and M. Otyepka, *J. Am. Chem. Soc.*, 2013, **135**, 6372–6377.
42 X. Wu, J. Dai, Y. Zhao, Z. Zhuo, J. Yang and X. C. Zeng, *ACS Nano*, 2012, **6**, 7443–7453.
43 M. Yao, Y. Ji, H. Wang, Z. Ao, G. Li and T. An, *J. Phys. Chem. C*, 2017, **121**, 13717–13722.
44 R. Q. Zhang, C.-E. Kim, B.-D. Yu, C. Stampfl and A. Soon, *Phys. Chem. Chem. Phys.*, 2013, **15**, 19450–19456.
45 J. Rossmeisl, J. K. Nørskov, C. D. Taylor, M. J. Janik and M. Neurock, *J. Phys. Chem. B*, 2006, **110**, 21833–21839.
46 Y.-J. Tak, S. Yang, H. Lee, D.-H. Lim and A. Soon, *J. Ind. Eng. Chem.*, 2018, **58**, 208–215.
47 I. C. Man, H.-Y. Su, F. Calle-Vallejo, H. A. Hansen, J. I. Martínez, N. G. Inoglu, J. Kitchin, T. F. Jaramillo, J. K. Nørskov and J. Rossmeisl, *ChemCatChem*, 2011, **3**, 1159–1165.
48 J. K. Nørskov, T. Bligaard, A. Logadottir, J. R. Kitchin, J. G. Chen, S. Pandelov and U. Stimming, *J. Electrochem. Soc.*, 2005, **152**, J23–J26.
49 L. Qi, W. Gao and Q. Jiang, *J. Phys. Chem. C*, 2020, **124**, 23134–23142.
50 Q. Xu, G. Li, Y. Zhang, Q. Yang, Y. Sun and C. Felser, *ACS Catal.*, 2020, **10**, 5042–5048.
51 N. Abidi, A. Bonduelle-Skrzypczak and S. N. Steinmann, *ACS Appl. Mater. Interfaces*, 2020, **12**, 31401–31410.
52 R. Shang, S. N. Steinmann, B. Q. Xu and P. Sautet, *Catal. Sci. Technol.*, 2020, **10**, 1006–1014.
53 V. Stamenkovic, B. S. Mun, K. J. J. Mayrhofer, P. N. Ross, N. M. Markovic, J. Rossmeisl, J. Greeley and J. K. Nørskov, *Angew. Chem., Int. Ed.*, 2006, **118**, 2963–2967.